Electron Bremsstrahlung Hard X-Ray Spectra, Electron Distributions and Energetics in the 2002 July 23 Solar Flare

Gordon D. Holman, Linhui Sui[1], and Richard A. Schwartz[2]

Laboratory for Astronomy and Solar Physics, Code 682, NASA/Goddard Space Flight Center, Greenbelt, MD 20771

holman@stars.gsfc.nasa.gov, lhsui@stars.gsfc.nasa.gov,
richard.schwartz@gsfc.nasa.gov

and

A. Gordon Emslie

Department of Physics, The University of Alabama in Huntsville, Huntsville, AL 35899

emslieg@uah.edu

ABSTRACT

We present and analyze the first high-resolution hard X-ray spectra from a solar flare observed in both X-ray/γ-ray continuum and γ-ray lines. The 2002 July 23 flare was observed by the Ramaty High Energy Solar Spectroscopic Imager (RHESSI). The spatially integrated photon flux spectra are well fitted between 10 and 300 keV by the combination of an isothermal component and a double power law. The flare plasma temperature peaks at 40 MK around the time of peak hard X-ray emission and remains above 20 MK 37 min later. We first derive the nonthermal mean electron flux distribution in one time interval by directly fitting the RHESSI X-ray spectrum with the thin-target bremsstrahlung from a double power-law electron distribution with a low-energy cutoff. We find that relativistic effects significantly impact the bremsstrahlung spectrum above 100 keV and, therefore, the deduced electron distribution. Next, we derive the evolution of the electron flux distribution on the assumption that the emission is thick-target bremsstrahlung. The injected nonthermal electrons are well described throughout the flare by this double power-law distribution with a low-energy cutoff that

---

[1] The Catholic University of America

[2] SSAI

is typically between 20–40 keV. Using our thick-target results, we compare the energy contained in the nonthermal electrons with the energy content of the thermal flare plasma observed by RHESSI and GOES. We find that the power in nonthermal electrons peaks before the impulsive rise of the hard X-ray and γ-ray emissions at 00:27 UT, and the minimum total energy deposited into the flare plasma by nonthermal electrons, 2.6×10^{31} erg, is on the order of the energy in the thermal plasma.

Subject headings: Sun: flares, Sun: X-rays, gamma rays

1. X-Ray Spectra

This *Letter* focuses on electrons in the 2002 July 23 solar flare. In this Section spatially integrated photon flux spectra and their time evolution are derived from Ramaty High Energy Solar Spectroscopic Imager (RHESSI) data in the 10–300 keV energy range. (The flare γ-ray bremsstrahlung above 300 keV is discussed in Share et al. 2003 and Smith et al. 2003.) In § 2 and § 3 these spectra are fitted with computations of the bremsstrahlung flux from model electron distribution functions to deduce the temporal evolution of the flare electrons. Our results are discussed in § 4.

The time history of the flare emission in three energy bands is shown in Figure 1a. RHESSI uses two sets of aluminum attenuators, known as thin shutters and thick shutters, to avoid saturating the detectors during large flares. The July 23 flare was observed in two attenuator states. The instrument was primarily in the A3 state, with both sets of attenuators in place. Early in the flare, before 00:26:08 UT, and late in the flare, after 00:59:21 UT, the instrument was in the A1 state, with only the thin shutters in place. There were also four brief periods during which the instrument switched from A3 to A1 and back to A3. These transitions in attenuator state are apparent in the time history of the lowest energy band in Fig. 1a. The flux calibration is currently uncertain during these four brief periods, so these time periods appear as gaps in subsequent results derived from the data.

Spectral fits were obtained using the Solar Software (SSW) spectral analysis routine (SPEX, see Schwartz 1996, Smith et al. 2002). Before fitting the data, we corrected the observed counts for pulse pileup and decimation (see Smith et al. 2002). Pulse pileup occurs at high count rates, with multiple photons being recorded as a single count with an energy equal to the sum of the energies of the individual photons. Decimation conserves onboard memory by recording only a fraction of the incident photons. Background counts were subtracted from the data by linearly interpolating between the background levels before and

after the flare.

Spectra obtained in the A1 state were fitted down to 10 keV photon energies, while spectra obtained in the A3 state were fitted down to 15 keV. This is because the attenuators substantially diminish the photon flux that reaches the RHESSI detectors at lower energies, and the calibration is currently not well established at these energies. The spectra were fitted up to 300 keV unless the contribution from background counts was significant below this energy. At times earlier than 00:26:00 UT, for example, spectral fits could not be obtained above 60 keV. We estimate the systematic uncertainty in the fluxes in each energy bin, which dominates the random (Poisson) noise at high count rates, to be 2% in the A3 state and 5% in the A1 state. The absolute uncertainty in the RHESSI flux measurements is currently unknown. These estimates were obtained by requiring the reduced χ^2 for our spectral fits to be on the order of one.

We have used a forward fitting procedure, for which we assume the spectral form of the incident flux. We used an isothermal bremsstrahlung spectrum plus a double power law, giving us 6 free parameters: the temperature (T) and emission measure (EM) of the isothermal component, lower (γ_L) and upper (γ_U) spectral indices and the photon energy at which the spectral break occurs ($\mathcal{E}_B$), and the normalization for the double-power-law spectrum, taken to be the photon flux at 50 keV (F_{50}). This is folded through the instrument response to provide the expected count rates. The free parameters are varied until a minimum χ^2 fit to the count rates is obtained.

During the early rise of the flare (A1 state), we found that the spectra could be fitted with a double power law alone. An equally good fit could be obtained with the combination of an isothermal component and a double power law above ∼18 keV. The results of this fit are shown in Fig. 1. Since this thermal component is not required by the data, the temperatures and emission measures derived from these fits are not as well established as those derived from fits for later time intervals when the thermal component is visually apparent in the spectra (as in Fig. 2). Late in the flare, only the isothermal component is evident. We expect to obtain a better determination of the thermal contribution to these spectra when RHESSI's response to the continuum radiation and iron-line complex below 10 keV are better understood.

The time history of the temperature of the isothermal component is shown in Fig. 1b (plus signs). The temperature rapidly rises to "superhot" values (Lin et al. 1981) as high as 40 MK. This hot thermal emission is consistent with the spectrum of the "coronal" source observed in RHESSI images (Emslie et al. 2003). The plasma gradually cools after the end of the first peak in the flare emission, with some reheating in subsequent peaks. The plasma temperature derived from the RHESSI spectra remains above 20 MK for at least

37 min after reaching its peak value. Temperatures derived from GOES data are shown for comparison (solid curve). Throughout the flare the temperatures derived from the RHESSI data are typically around 10 MK higher than those derived from the GOES data. These higher temperatures are expected for a multithermal plasma, since RHESSI is sensitive to higher photon energies than GOES.

The emission measure of the isothermal component is plotted in Fig. 1c (plus signs). Although the peak temperature is similar to that obtained by Lin et al. (1981) for the 1980 June 27 flare, the peak emission measure is thirty times greater, consistent with the higher X-ray intensity of this flare. The GOES emission measure (solid curve, scaled by a factor of 0.25) always exceeds the RHESSI emission measure, as expected for the lower temperatures obtained from GOES.

The spectral indices γ_L and γ_U, defined by Flux $\propto \mathcal{E}^{-\gamma}$, have values between 2.5 and 3.5 throughout most of the flare (Fig. 1d). These spectral indices and their time evolution are consistent with the spectra obtained for the "footpoint" sources observed in RHESSI images (Emslie et al. 2003). Earlier in the flare, before the impulsive rise at 00:27:00 UT, the spectral indices are much greater, on the order of 5 and 6.5. While $\Delta\gamma$ is between 1 and 2 before the impulsive rise, it is subsequently 0.5 or less. When the nonthermal spectrum is observable after 00:40:00 UT, it is best fit with a single power law. The break energy, plotted in Fig. 1e, increases from values below 50 keV before the impulsive rise of the flare to values in the range 70–125 keV afterwards. The time history of the photon flux at 50 keV is plotted in Fig. 1f. This closely follows the 40–100 keV light curve, as expected.

2. Mean Electron Flux Distribution

The mean electron flux distribution (electrons cm^{-2} s^{-1} keV^{-1}) is the spatially averaged value of the electron flux weighted by the plasma density (Brown, Emslie & Kontar 2003). This distribution is independent of any assumptions regarding the evolution of electrons in the source and, therefore, is well suited for comparison with electron distributions computed from theoretical flare models. Deducing the mean electron flux from a photon spectrum is equivalent to deducing the electron flux under the assumption that the radiation is thin-target bremsstrahlung from a spatially homogeneous electron flux distribution.

In this paper, we deduce the mean electron flux distribution for the time interval 00:30:00–00:30:20 UT (see Fig. 1a), for comparison with the result of Piana et al. (2003) and Kontar et al. (2003). Piana et al. derive the mean electron flux distribution for this same time interval using a regularized, direct inversion procedure, while Kontar et al. in-

clude nonuniform target ionization in their spectral fit. We obtain our result by assuming that the functional form of the mean electron flux distribution is a double power law (power-law index δ_L below a break energy E_B, δ_U above) with a low-energy cutoff (E_c). We fit the observed count-rate spectrum in the 15–300 keV photon energy range with the bremsstrahlung spectrum computed from this distribution and an isothermal bremsstrahlung distribution, using the same SPEX forward fitting technique described in § 1. The result of our 7-parameter fit is shown in Figure 2. For this and subsequent computations in § 3, the relativistic bremsstrahlung cross section of Haug (1997) is used with the Elwert (1939) correction.

The spectral fit is shown in the top panel of Figure 2. The best-fit parameters are provided in the figure caption. Plotted in the center panel are the residuals from this fit, defined as $(F_{obs}(\mathcal{E}) - F_{fit}(\mathcal{E}))/\sigma(\mathcal{E})$, where $\mathcal{E}$ is the photon energy, F_{obs} is the observed photon flux, F_{fit} is the photon flux given by the model at energy $\mathcal{E}$, and σ is the uncertainty in the observed flux. The uncertainty σ includes both the systematic uncertainty, discussed in Section 1, and the Poisson statistics, added in quadrature. The residuals are limited to about the $\pm 2\sigma$ level. In the bottom panel the mean electron flux distribution is plotted as a function of electron energy. The fit to the photon flux spectrum actually provides the quantity $\overline{n} V \overline{F}(E)$, where V is the volume of the emitting region, $\overline{n}$ is the mean density of the thermal plasma in the emitting volume, and $\overline{F}(E)$ is the mean electron flux distribution, so this is what is plotted. In the third fit parameter, $\overline{F}$ is the mean electron flux distribution integrated from E_c to the highest electron energy in the distribution (we used a value of 5 MeV).

The break energy, E_B, for the electron distribution is higher than that for the photon spectrum ($\mathcal{E}_B = 77$ keV) because bremsstrahlung photons are produced by electrons with higher energies than the photon energy. The photon spectrum below E_c flattens to about $\mathcal{E}^{-1}$. The power-law indices $\delta_L = 1.5$ and $\delta_U = 2.5$ for the mean electron flux distribution are smaller than the photon spectral indices $\gamma_L = 2.8$ and $\gamma_U = 2.9$, but not by 1 as predicted for nonrelativistic, thin-target bremsstrahlung from a single power-law electron flux distribution. For this relatively flat electron distribution, relativistic flattening of the bremsstrahlung spectrum is important at photon energies above 100 keV. Therefore, δ_U is larger than 1.9 to compensate for the fact that the observed spectrum does not flatten above 100 keV. To prevent the photon spectrum from being too steep below 100 keV, δ_L is somewhat less than 1.8.

The result of Piana et al. using the regularized, direct inversion procedure is quite similar to ours, but shows a dip in the mean electron flux distribution between 50 and 60 keV. Kontar et al. find that injection of the electrons into a nonuniformly ionized target plasma, which

flattens the bremsstrahlung spectrum below an effective break energy, provides a better fit to the spectrum than a single power-law distribution. All three distributions provide an acceptable χ^2 fit to the photon spectrum. The differences in these derived electron distributions highlight the fact that there is not a unique electron distribution associated with an observed count-rate spectrum. The residuals of all three fits show some systematic variation with photon energy, especially below ~30 keV. We are currently exploring whether these residuals contain enough information to distinguish the different fits at a statistically significant level.

3.   Thick-Target Flux Distributions and Energetics

Electron flux distributions (electrons s^{-1} keV^{-1}) are derived on the assumption that the nonthermal hard X-ray emission is thick-target bremsstrahlung (Brown 1971) and that the electron distribution is a double power law with a low-energy cutoff. The thick-target bremsstrahlung from this electron distribution is numerically computed and added to an isothermal bremsstrahlung component. The resulting photon spectra, determined by 7 free parameters, are fitted to the RHESSI count-rate spectra. The results are shown in Figure 3.

The upper electron power-law indices (triangles, Fig. 3b) are larger by about one than the upper photon spectral indices, as expected ($\delta_U \simeq \gamma_U + 1$). (The relativistic flattening of the bremsstrahlung spectrum is not as prominent for thick-target emission as it is for thin-target emission.) The lower power-law indices are only slightly steeper than the lower photon indices, however, because fewer electrons are present above the break energy than would have been present for a single power law. The break energy (Fig. 3c) increases with time from values around 30 keV to values in excess of 200 keV. Before 00:23:20 UT and after 00:40:00 UT, the spectra were best fit with the isothermal component and a single power law with a low-energy cutoff. For most of the spectra after 00:40:00 UT, as with the photon fits (§ 1), only the isothermal component was evident.

The low-energy cutoff (Fig. 4d) minimizes the energy in nonthermal electrons. Except for the brief period between 00:40:40 UT and 00:42:00 UT, when the low-energy cutoff was as high as 73 keV, the low-energy cutoff is near the photon energy at which the isothermal (exponential) photon spectrum flattens to the nonthermal power-law spectrum. We note that this location for the low-energy cutoff is comparable to that obtained with a hybrid thermal/nonthermal electron acceleration model in which the hot flare plasma and a tail of runaway electrons are produced simultaneously (Holman & Benka 1992, Benka & Holman 1994). The low-energy cutoff increases from around 20 keV before 00:26:00 UT to 30–40 keV after this time.

The distributions before 00:26:00 UT are also consistent with a double power law alone and no isothermal component. We could also fit them with a single power law with a high energy cutoff (no isothermal component). The high-energy cutoff increases from 40 keV at early times to as high as 100 keV at later times. However, we found that these spectra could not be adequately fit with only a single power law with a low-energy cutoff (no isothermal component) or with an isothermal distribution alone.

The total electron flux, integrated over all electron energies, is plotted in Fig. 4e. It reaches its maximum value of 5×10^{36} electrons s^{-1} at 00:25:20 UT. Note that this is before the impulsive rise after 00:27:00 UT and the appearance of the much harder X-ray spectra and the γ-ray line emission.

We can estimate the total density of nonthermal electrons by dividing the flux distribution function by the electron speed and the area of the thick-target interaction region and integrating over all electron energies. We first obtain a lower limit on the density at the time of peak electron flux by assuming that the entire source area is thick target. Using the RHESSI image of Krucker et al. (2003) at 00:23:45 UT (their Fig. 1b) we estimate an area of 10^{19} cm^2. This gives a density in suprathermal electrons of 6×10^7 cm^{-3} at 00:25:20 UT. The nonthermal source area later in the flare has been estimated by White et al. (2003) to be 10^{17} cm^2. This gives densities that are up to an order of magnitude higher. In interpreting their radio observations of the flare, White et al. deduce a nonthermal electron density of 10^{11} cm^{-3} above 10 keV at 00:35:00 UT. We obtain a density of 3×10^9 cm^{-3} at this time if the electron distribution extends down to 10 keV. Most of the difference in these densities can be attributed to the flattening of the electron distribution below the break energy of 134 keV in our fit. If we were to extrapolate the part of the electron distribution that is relevant to the optically-thin radio observations, that above the break energy, down to 10 keV, the inferred density would be 2.4×10^{10} cm^{-3}.

The energy flux (solid curve with plus signs) and the total accumulated energy deposited into the flare plasma (dotted curve) by electrons with energies above E_c are plotted as a function of time in Fig. 4f. The energy flux (power) is obtained by multiplying the electron flux distribution derived for each 20-s interval times the electron energy and integrating over all energies above E_c. The accumulated energy is obtained by multiplying the energy flux at each time by the time interval (20 s) and obtaining the sum of these energies up to the time of interest. Note that about two-thirds of this energy is deposited before 00:26:00 UT. The total energy injected by these electrons during the whole flare is found to be 2.6×10^{31} erg.

The energies contained in the thermal plasmas observed by RHESSI (dot-dash line) and by GOES (solid line) are also plotted in Fig. 4f. Using the temperatures and emission measures derived from the observations, we are able to compute the product of the plasma

density and energy, $n(3nkTV)$. We can also estimate the volume (V) of the thermal plasma observed by RHESSI from the RHESSI images and, using the emission measure (EM), derive the density $n = \sqrt{EM/V}$. Before 00:27:00 UT we use the total source area in Fig. 1b (also, 1c) of Krucker et al. (2003) to estimate the volume to be 2×10^{28} cm^3. After 00:27:00 UT, during the main phase of the flare, we obtain 4×10^{27} cm^3 using the area of the coronal source in Fig. 1d (also, 1e) of Krucker et al. For an emission measure of 5×10^{49} cm^{-3}, for example, typical of the main phase of the flare (Fig. 1c), we obtain a density of 1×10^{11} cm^{-3} for the hot plasma observed by RHESSI. Writing the plasma energy as $3kT\sqrt{EM \cdot V}$, we use these volumes for both RHESSI and GOES to obtain the curves plotted in the figure.

We see from Fig. 4f that, even with the low-energy cutoffs derived here, the accumulated energy in the nonthermal electrons is comparable to the energy in the thermal plasma observed by both RHESSI and GOES. The peak energy in the thermal plasmas, 6.6×10^{30} erg for RHESSI and 1.1×10^{31} erg for GOES, is reached at about 00:36:00 UT. The energy deposited by the nonthermal electrons may be somewhat less than the energy in the thermal plasma if the volume of the plasma observed by GOES is at least ~ 4 times greater than the volume of the hotter plasma observed by RHESSI. (Since GOES did not provide images, we have no direct estimate of the volume of the plasma observed by GOES.) Otherwise, the energy is equal to or exceeds the thermal energy. Although we cannot determine from these results whether the energy contained in the nonthermal electrons was greater than or less than the energy in the hot thermal plasma, it is nevertheless significant that they are comparable, despite our spectral fits which minimize the energy in the nonthermal electrons.

Electron distributions with low-energy cutoffs lower than the values derived here are also consistent with the RHESSI spectra. Therefore, the energy deposited by the nonthermal electrons may be greater. Emslie (2003) shows that the temperature of the target plasma limits the energy that can be deposited into the plasma. The energy injected into the plasma is significantly less than the electron energy computed above a low-energy cutoff if the cutoff energy is less than $5kT$, where T is the temperature of the target plasma. Taking the temperature of the target plasma to be equal to or less than the temperatures we derived from the spectral fits, the low-energy cutoffs derived here all exceed $5kT$. Therefore, the computed injection energies are accurate unless undetected higher temperatures are present in the interaction region. Using our derived temperatures and the results of Emslie, we can compute the maximum energy these electrons could have injected into the flare plasma. We find this to be 4×10^{34} erg. It is unlikely that the electrons deposited this much energy into the flare plasma, since it is greater than the maximum total energy that has been deduced previously for even the largest solar flares.

4.   Conclusions

The RHESSI spectra presented and analyzed here are the most detailed hard X-ray spectra ever obtained for a large flare. Although these spectra are well fitted by isothermal (exponential) and double power-law photon distributions, fitting these spectra with the bremsstrahlung spectra computed from model electron distributions is an important part of our analysis. The electron distributions allow a more physical interpretation of the data and smooth out the unphysically sharp break in the double power-law photon spectrum. Even fits with a double power-law electron distribution, however, show systematic residuals at the level of a few percent, as in Fig. 3b. Understanding these residuals will also be an important part of the future analysis of RHESSI spectra.

The July 23 flare hard X-ray spectral data provide support for the longstanding impression that the energy in accelerated electrons is a major part of the energy released in many, if not all, flares. Our result for the energy injected by nonthermal electrons depends, however, on our nonthermal, thick-target interpretation of the double power-law fits. One compelling alternative is that the X-ray emission observed in the early rise phase of the flare (before 00:26:00 UT) is, at least in part, thin-target bremsstrahlung from the corona (Lin et al. 2003). The extended size of the X-ray source at this time is suggestive of this interpretation. However, this is likely to increase, rather than decrease, the total energy in nonthermal electrons. We note that if the flattening of the spectra below $\mathcal{E}_B$ is due to partial ionization in the target rather than a break in the electron distribution, the energy in nonthermal electrons increases. Another possibility is that the emission is from a multithermal plasma, but temperatures exceeding 100 MK would be required for this interpretation. A study of these alternatives requires additional modeling beyond the scope of this paper.

The information extracted from these spatially integrated spectra can only be fully appreciated and understood through comparison with RHESSI images and imaged spectra, and with related observations of the flare. A synthesis of the overall flare data and a discussion of possible interpretations are contained in Lin et al. (2003).

REFERENCES

Benka, S. G. & Holman, G. D. 1994, ApJ, 435, 469

Brown, J. C. 1971, Sol. Phys., 18, 489

Brown, J. C., Emslie, A. G. & Kontar, E. P. 2003, ApJ, this issue

Elwert, G. 1939, Ann. Physik, 34, 178

Emslie, A. G. 2003, ApJ, this issue

Emslie, A. G., Kontar, E. P., Krucker, S. & Lin, R. P. 2003, ApJ, this issue

Haug, E. 1997, A&A, 326, 417

Holman, G. D. & Benka, S. G. 1992, ApJ, 400, L79

Kontar, E. P., Emslie, A. G., Krucker, S. & Lin, R. P. 2003, ApJ, this issue

Krucker, S., Hurford, G. J. & Lin, R. P. 2003, ApJ, this issue

Lin, R. P., Schwartz, R. A., Pelling, R. M. & Hurley, K. C. 1981, ApJ, 251, L109

Lin, R. P., et al. 2003, ApJ, this issue

Piana, M., Massone, A. M., Kontar, E. P., Emslie, A. G., Brown, J. C. & Schwartz, R. A. 2003, ApJ, this issue

Schwartz, R. A. 1996, "Compton Gamma Ray Observatory Phase 4 Guest Investigator Program: Solar Flare Hard X-ray Spectroscopy," Technical Report, NASA Goddard Space Flight Center

Share, G., Murphy, R. J., Lin, R. P., Smith, D. M. & Schwartz, R. A. 2003, ApJ, this issue

Smith, D., et al. 2002, Sol. Phys., 210, 33

Smith, D. M., Share, G. H., Murphy, R. J., Schwartz, R. A., Shih, A. Y., & Lin, R. P. 2003, ApJ, this issue

White, S. M., Krucker, S., Shibasaki, K., Yokoyama, T., Shimojo, M. & Kundu, M. R. 2003, ApJ, this issue
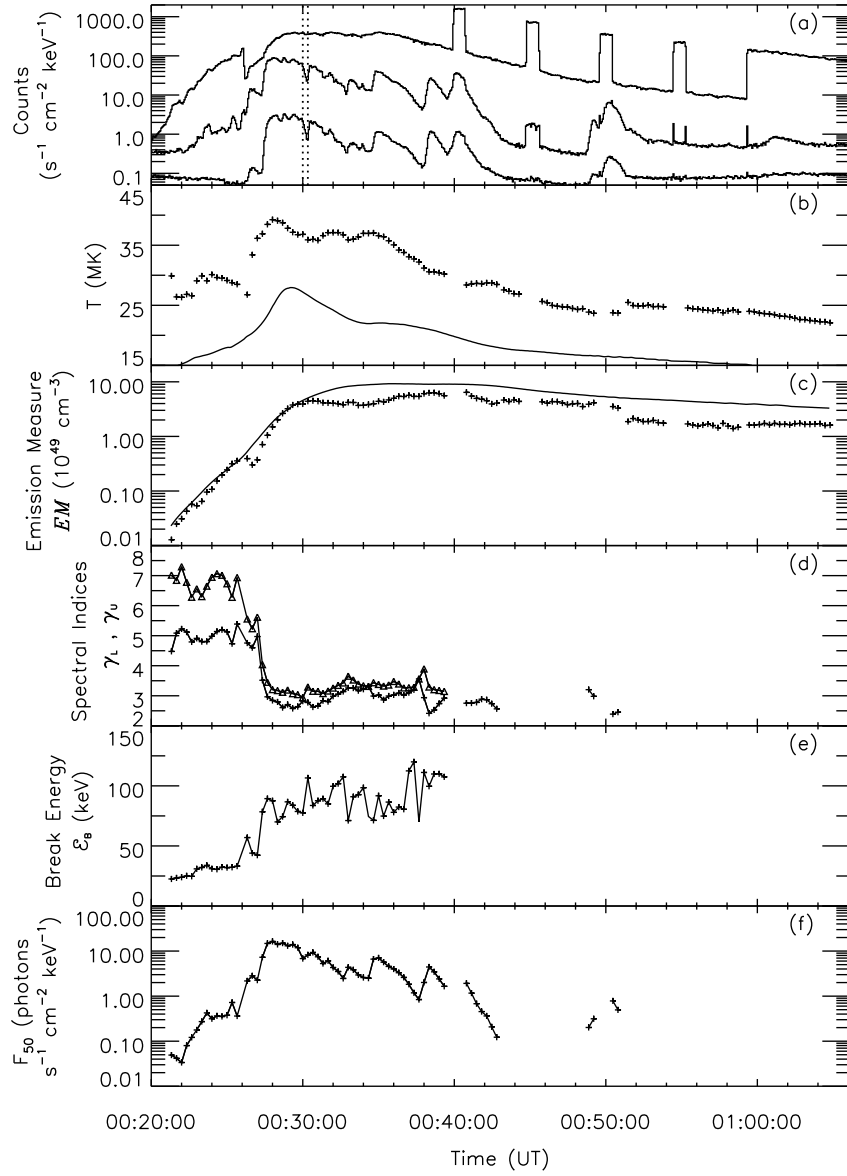
Fig. 1.— RHESSI X-ray light curves and time history of fit parameters. (a) Light curves in three energy bands, scaled to avoid overlap. The energy bands and scale factors are 12–40 keV (*top curve*, ×0.6), 40–100 keV (*middle curve*, ×3), and 100–300 keV (*bottom curve*, ×1). The *dotted vertical lines* show the beginning and end of the integration time interval for the spectrum in Fig. 2. (b) Time history of the temperature of the isothermal component (20-s time resolution, *plus signs*). The *solid curve* is the temperature derived from GOES data. (c) Time history of the isothermal emission measure (*plus signs*). The *solid curve* is the emission measure derived from GOES data, scaled by a factor of 0.25. (d) Time history of the double power-law spectral indices (spectral index below break, *plus signs*; spectral index above break, *triangles*). (e) Time history of the break energy in the double power-law spectra. (f) Time history of the photon flux at 50 keV, determined from the double power-law fit.
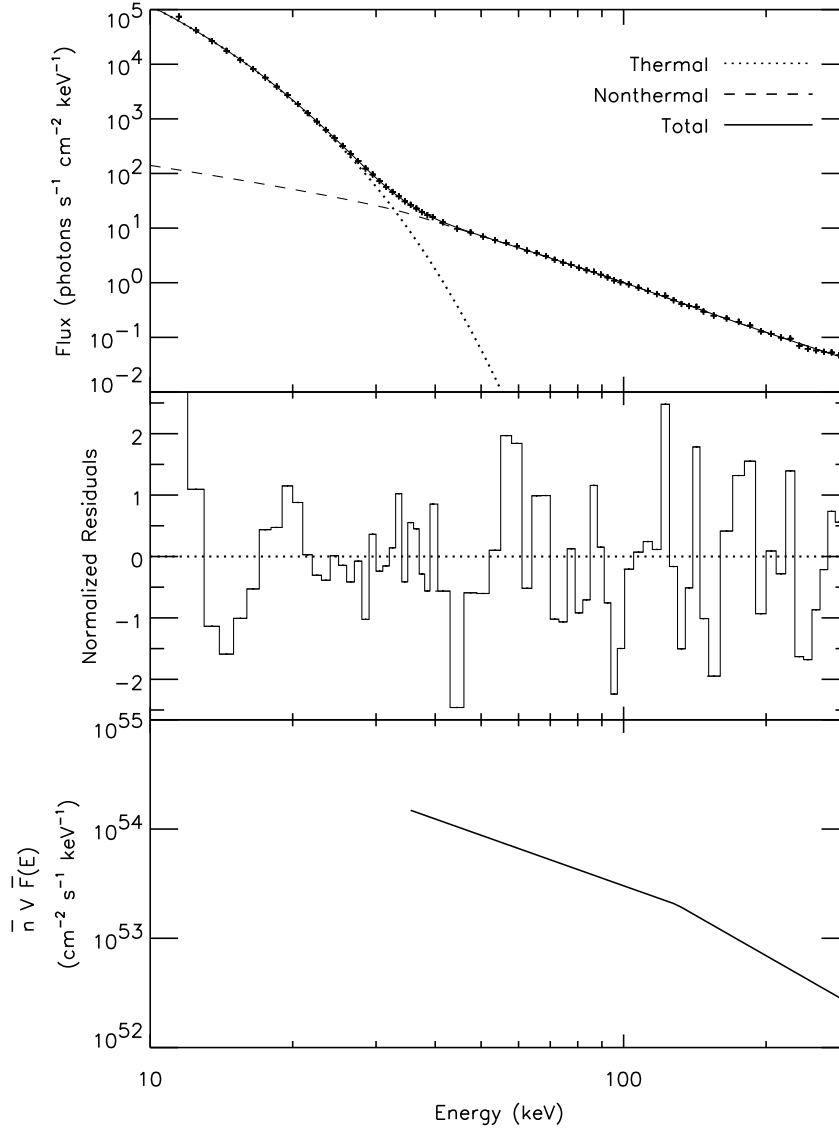
Fig. 2.— Mean electron flux fit and residuals for the 00:30:00–00:30:20 UT time interval. The fit to the photon flux (*plus signs*) in the *upper panel*, plotted as a function of photon energy in keV, is the bremsstrahlung from an isothermal plasma (*dotted curve*) and a double power-law mean electron flux distribution with a low-energy cutoff (*dashed curve*). The *solid curve* is the total fit. The best fit parameters were $EM = 4.1 \times 10^{49}$ cm^{-3}, $T = 37$ MK, $\overline{nV}\overline{F} = 6.9 \times 10^{55}$ cm^{-2} s^{-1}, $E_c = 34$ keV, $\delta_L = 1.5$, $E_B = 129$ keV, and $\delta_U = 2.5$ with a reduced χ^2 of 0.94. The residuals in the *center panel* are defined as the observed flux minus the model flux divided by the estimated one sigma uncertainty in each data point. The *bottom panel* shows the mean electron flux distribution times $\overline{n}V$, plotted as a function of electron energy in keV.
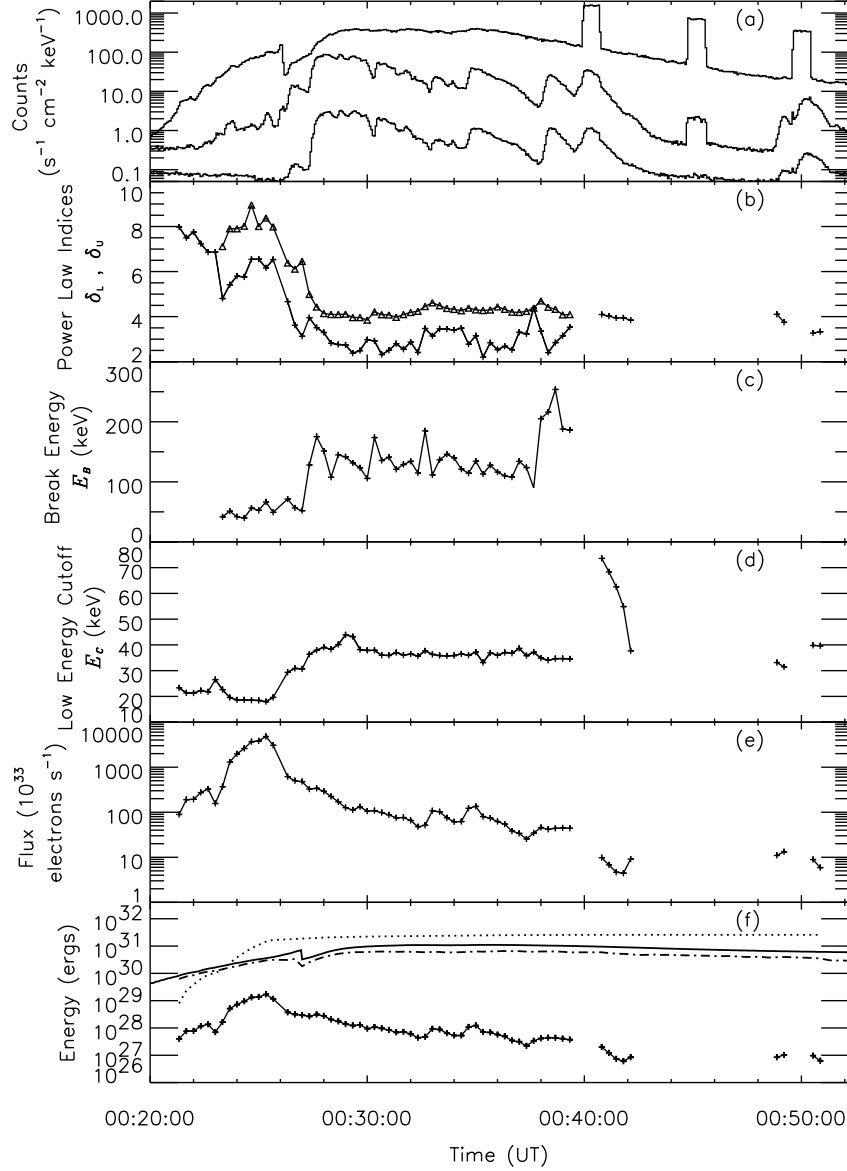
Fig. 3.— Thick-target bremsstrahlung electron flux distribution fit parameters and energetics. (a) X-ray light curves in three energy bands (see Fig. 1a). (b) Time history of the upper and lower power-law indices (20-s time resolution, same symbols as Fig. 1d). (c) Time history of the break energy in the double power-law electron flux distribution. (d) Time history of the low-energy cutoff in the electron flux distribution. (e) Time history of the integrated (over all electron energies) electron flux. (f) Thermal and nonthermal energetics. The time history of the energy in the GOES (*solid line*) and RHESSI (*dot-dash line*) isothermal fits is plotted using volumes estimated from RHESSI images (see text). This is compared to the accumulated energy in nonthermal electrons (*dotted curve*). The lower curve, marked with *plus signs*, is the energy injection rate (erg s^{-1}).